RESEARCH BRIEF

Radiotherapy and Immunotherapy Promote Tumoral Lipid Oxidation and Ferroptosis via Synergistic Repression of SLC7A11

Xueting Lang[1,2,3], Michael D. Green[2,3], Weimin Wang[1,2], Jiali Yu[1,2], Jae Eun Choi[2,4,5], Long Jiang[2,3], Peng Liao[1,2], Jiajia Zhou[1,2], Qiang Zhang[2,3], Ania Dow[1], Anjali L. Saripalli[6], Ilona Kryczek[1,2], Shuang Wei[1,2], Wojciech Szeliga[1,2], Linda Vatan[1,2], Everett M. Stone[7,8], George Georgiou[7,8], Marcin Cieslik[4,9,10], Daniel R. Wahl[3], Meredith A. Morgan[3], Arul M. Chinnaiyan[4,5,9,10], Theodore S. Lawrence[3], and Weiping Zou[1,2,4,11,12]

ABSTRACT

A challenge in oncology is to rationally and effectively integrate immunotherapy with traditional modalities, including radiotherapy. Here, we demonstrate that radiotherapy induces tumor-cell ferroptosis. Ferroptosis agonists augment and ferroptosis antagonists limit radiotherapy efficacy in tumor models. Immunotherapy sensitizes tumors to radiotherapy by promoting tumor-cell ferroptosis. Mechanistically, IFNγ derived from immunotherapy-activated $CD8^+$ T cells and radiotherapy-activated ATM independently, yet synergistically, suppresses SLC7A11, a unit of the glutamate–cystine antiporter xc^-, resulting in reduced cystine uptake, enhanced tumor lipid oxidation and ferroptosis, and improved tumor control. Thus, ferroptosis is an unappreciated mechanism and focus for the development of effective combinatorial cancer therapy.

SIGNIFICANCE: This article describes ferroptosis as a previously unappreciated mechanism of action for radiotherapy. Further, it shows that ferroptosis is a novel point of synergy between immunotherapy and radiotherapy. Finally, it nominates SLC7A11, a critical regulator of ferroptosis, as a mechanistic determinant of synergy between radiotherapy and immunotherapy.

INTRODUCTION

Immune checkpoint blockade is a powerful oncologic treatment modality for a wide variety of human malignancies (1). Randomized clinical trials are assessing how best to interdigitate this treatment modality with traditional therapies including radiotherapy (2). Thus far, preclinical data have suggested that immune checkpoint blockade can synergize with

[1]Department of Surgery, University of Michigan Rogel Cancer Center, Ann Arbor, Michigan. [2]Center of Excellence for Cancer Immunology and Immunotherapy, University of Michigan Rogel Cancer Center, Ann Arbor, Michigan. [3]Department of Radiation Oncology, University of Michigan School of Medicine, Ann Arbor, Michigan. [4]Department of Pathology, University of Michigan School of Medicine, Ann Arbor, Michigan. [5]Michigan Center for Translational Pathology, University of Michigan School of Medicine, Ann Arbor, Michigan. [6]Department of Medical Education, University of Michigan School of Medicine, Ann Arbor, Michigan. [7]Department of Chemical Engineering, The University of Texas at Austin, Austin, Texas. [8]Department of Molecular Biosciences, The University of Texas at Austin, Austin, Texas. [9]Department of Computational Medicine and Bioinformatics, University of Michigan School of Medicine, Ann Arbor, Michigan. [10]Howard Hughes Medical Institute, University of Michigan School of Medicine, Ann Arbor, Michigan. [11]Graduate Program in Immunology, University of Michigan School of Medicine, Ann Arbor, Michigan. [12]Graduate Program in Cancer Biology, University of Michigan School of Medicine, Ann Arbor, Michigan.

Note: Supplementary data for this article are available at Cancer Discovery Online (http://cancerdiscovery.aacrjournals.org/).

X. Lang and M.D. Green contributed equally to this article.

Corresponding Author: Weiping Zou, University of Michigan School of Medicine, BSRB 5071, 109 Zina Pitcher Place, Ann Arbor, MI 48109. Phone: 734-763-6402; Fax: 734-763-0143; E-mail: wzou@umich.edu

Cancer Discov 2019;9:1673–85

doi: 10.1158/2159-8290.CD-19-0338

radiotherapy through agonism of innate immune sensing pathways activated as a consequence of DNA damage (3–5).

It is well established that unrepaired DNA double-strand breaks dictate cellular survival following radiotherapy (6). These lesions promote mitotic catastrophe, an unregulated form of cell death (7). More recent examinations have implicated a number of other forms of regulated cell death, including apoptosis, necroptosis, and autophagy in the response to radiotherapy (8, 9). Radiotherapy stochastically induces oxidative damage in all cellular compartments, including the lipid membrane (10, 11). Toxic lipid peroxidation accumulation has only recently been implicated in directly causing a regulated form of cell death, termed ferroptosis (12). The sources of cell death–inducing reactive oxygen species (ROS) that predispose cells to undergo ferroptosis have not been defined. It has been suggested that radiation-induced lipid oxidation results in apoptosis (13), but the relationship between radiotherapy and ferroptosis remains undefined. Further, radiotherapy efficacy *in vivo* is dependent on the presence of $CD8^+$ T cells (14, 15). We have recently discovered that $CD8^+$ T cells modulate tumoral ferroptosis through IFNγ (16). It is unknown if ferroptosis underlies the interplay between the adaptive immune system and radiotherapy.

To address these questions, we explored the involvement of lipid peroxidation and ferroptosis in response to radiotherapy. We implicate ferroptosis as a previously unknown mechanism of tumor cell death following radiotherapy *in vitro* and *in vivo*. In addition, we have found that radiotherapy can sensitize tumor cells to ferroptosis agonists *in vitro* and *in vivo*, highlighting a novel strategy to radiosensitize tumors. Moreover, we have implicated ferroptosis as a direct link through which $CD8^+$ T cells and radiotherapy cooperate to improve tumor control. Mechanistically, IFNγ derived from immunotherapy-activated $CD8^+$ T cells and ATM activated following radiotherapy synergistically suppress SLC7A11, a unit of the glutamate–cystine antiporter xc^-, resulting in enhanced tumor lipid oxidation and ferroptosis. This work is the first to nominate radiotherapy as a therapeutic ferroptosis inducer and suggest ferroptosis agonists as a novel class of sensitizers for radiotherapy and immunotherapy. Finally, our studies highlight lipid peroxidation as a previously unappreciated point of mechanistic interplay between radiotherapy and immunotherapy in cancer.

RESULTS

Radiotherapy Induces Tumor-Cell Ferroptosis

Ferroptosis is a recently discovered form of cell death that differs from apoptosis and results from iron-dependent lipid peroxide accumulation (12, 17). It is unknown whether lipid oxidation and ferroptosis are induced by radiotherapy. To test this *in vivo*, we inoculated ID8 ovarian cancer cells into the peritoneal cavity of C57BL/6 mice and treated the mice with a single dose of 8 Gray (Gy) ionizing radiation, liproxstatin-1, a ferroptosis antagonist, or both agents concurrently. ID8 tumor–bearing mice tolerated radiotherapy without changes in mouse weight (Supplementary Fig. S1A). Radiotherapy, but not liproxstatin-1, reduced tumor growth (Fig. 1A). Unexpectedly, liproxstatin-1 administration concurrent and adjuvant to radiotherapy diminished radiotherapy efficacy (Fig. 1A).

To extend this finding, we inoculated B16F10 melanoma cells into C57BL/6 mice and allowed the tumors to establish. Subsequently, B16F10-bearing mice were treated with a single fraction of 8 Gy. Again, radiotherapy reduced tumor growth (Supplementary Fig. S1B). Dual treatment with liproxstatin-1 and radiotherapy partially and significantly abrogated radiotherapy efficacy. Ferroptosis is accompanied by increased lipid peroxidation, which can be examined using the lipophilic redox-sensitive dye C11BODIPY (12). C11BODIPY quantification showed that radiotherapy increased lipid peroxidation *in vivo*, and concurrent liproxstatin-1 treatment abrogated radiotherapy-induced lipid peroxidation in B16F10 tumors (Fig. 1B; Supplementary Fig. S1C).

To orthogonally confirm that tumoral ferroptosis occurs following radiotherapy, we generated ferroptosis-resistant subclones of B16F10 through serial exposure to RSL-3, a ferroptosis agonist. We showed that RSL-3–resistant B16F10 cells were indeed resistant to RSL-3 and erastin, two ferroptosis agonists (Supplementary Fig. S1D). We then inoculated parental or RSL-3–resistant B16F10 cells into C57BL/6 mice and treated established tumors with radiotherapy. We observed that resistance to ferroptosis significantly reduced the efficiency of radiotherapy (Fig. 1C). Further, RSL-3–resistant tumors failed to manifest a robust increase in lipid peroxidation following radiotherapy as compared with parental tumors (Fig. 1D). We additionally generated ferroptosis-resistant ID8 subclones through serial exposure to erastin. We also showed that erastin-resistant ID8 cells were resistant to RSL-3 and erastin (Supplementary Fig. S1E). We inoculated parental and erastin-resistant ID8 cells into C57BL/6 mice and treated established ID8 tumors with radiotherapy. Again, we observed reduced radiotherapy efficacy in erastin-resistant tumors (Fig. 1E). Together, these data suggest that radiotherapy induces tumor ferroptosis and also that ferroptosis is critical for radiotherapy efficacy.

To understand whether radiotherapy directly induces tumor ferroptosis, we performed clonogenic survival assays following radiotherapy in HT1080 human fibrosarcoma cells *in vitro*. We observed that ferroptosis inhibitors liproxstatin-1 and ferrostatin-1, the lipophilic antioxidant trolox, and the iron chelator deferoxamine (DFO) increased clonogenic cell survival following radiotherapy (Fig. 1F). To determine whether radiotherapy directly affected lipid peroxidation, we conducted C11BODIPY staining in HT1080 cells *in vitro*. We observed that radiotherapy resulted in an increase in lipid ROS in HT1080 cells (Fig. 1G). We next examined clonogenic cell survival and lipid peroxidation in B16F10 and ID8 cells. Again, liproxstatin-1, as well as trolox and DFO, enhanced clonogenic survival in B16F10 (Supplementary Fig. S1F) and ID8 (Supplementary Fig. S1G) cells following radiotherapy. Radiotherapy induced an increased lipid peroxidation in B16F10 cells (Supplementary Fig. S1H) and ID8 cells (Supplementary Fig. S1I) in a dose-dependent manner. These results suggest that radiotherapy directly induces tumor ferroptosis.

Given that radiotherapy can induce tumor ferroptosis (Fig. 1A–G; Supplementary Fig. S1A–S1I), we wondered whether ferroptosis agonists could enhance radiotherapy efficacy and be exploited as novel radiosensitizers. To explore this possibility,

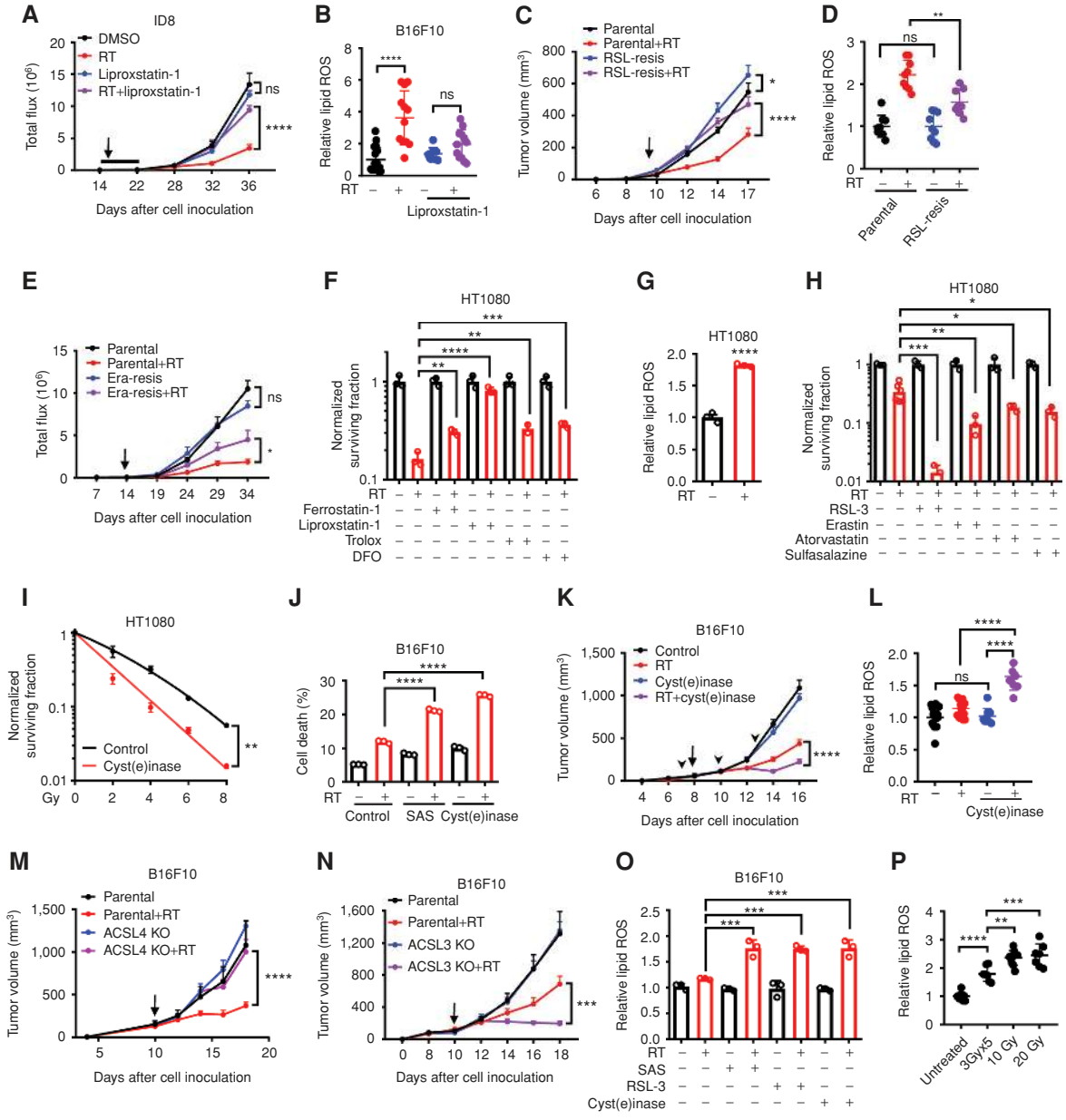

Figure 1. Radiotherapy induces tumor cell ferroptosis. **A,** ID8 tumor growth following radiotherapy (RT; 8 Gy, single fraction, arrow) and/or liproxstatin-1 treatment (50 mg/kg, administered daily for 5 days, bar) *in vivo*. $n = 10$ per group, ns, $P > 0.05$; ****, $P < 0.0001$, two-way ANOVA. **B,** B16F10 tumor lipid ROS levels following radiotherapy (8 Gy, single fraction) and/or liproxstatin-1 treatment (50 mg/kg, administered daily for 5 days) *in vivo*. DMSO, $n = 17$; RT, $n = 14$; liproxstatin-1, $n = 10$; RT+liproxstatin-1, $n = 12$, ns, $P > 0.05$; ****, $P < 0.001$, two-way ANOVA. **C** and **D,** RSL-3–resistant (RSL-resis) B16F10 (**C**) tumor growth *in vivo* and (**D**) tumor lipid ROS levels following radiotherapy (8 Gy, single fraction, arrow). $n = 14$ per group; **C,** ****, $P < 0.0001$, two-way ANOVA; **D,** ns, $P > 0.05$; **, $P < 0.01$, two-way ANOVA. **E,** Erastin-resistant (Era-resis) ID8 tumor growth following radiotherapy (8 Gy, single fraction, arrow) *in vivo*. $n = 10$ per group, ns, $P > 0.05$; *, $P < 0.05$, two-way ANOVA. **F,** Clonogenic survival of HT1080 cells treated with DMSO, ferrostatin-1 (5 μmol/L), liproxstatin-1 (5 μmol/L), trolox (200 μmol/L), or DFO (2 μmol/L) as indicated and then irradiated (6 Gy) *in vitro*. Representative biological triplicate shown, mean ± SD. ****, $P < 0.0001$, one-way ANOVA. **G,** HT1080 lipid ROS levels *in vitro* following radiotherapy (8 Gy) *in vitro*. Representative biological triplicates shown, mean ± SD. ****, $P < 0.0001$, unpaired Student *t* test. **H,** Clonogenic survival of HT1080 cells following treatment with DMSO, RSL-3 (0.05 μmol/L), erastin (2 μmol/L), atorvastatin (5 μmol/L), or sulfasalazine (5 μmol/L) as indicated and radiotherapy (4 Gy) *in vitro*. Representative biological triplicate shown, mean ± SD. *, $P < 0.05$; **, $P < 0.01$; ***, $P < 0.001$, one-way ANOVA. **I,** Clonogenic survival of HT1080 cells at indicated radiotherapy dose following cyst(e)inase (10 μmol/L) treatment *in vitro*. Representative biological triplicates shown, mean ± SD. **, $P < 0.005$, unpaired Student *t* test. **J,** B16F10 cell death following sulfasalazine (SAS; 5 μmol/L) or cyst(e)inase (10 μmol/L) and irradiation (20 Gy) *in vitro*. ****, $P < 0.0001$, two-way ANOVA. **K** and **L,** B16F10 tumor growth (**K**) and tumor lipid ROS levels (**L**) following radiotherapy (8 Gy, one fraction, arrow) and/or cyst(e)inase (87.5 mg/kg, arrowhead) *in vivo*. $n = 10$ per group, ns, $P > 0.05$; ****, $P < 0.0001$, two-way ANOVA. **M,** ACSL4 knockout (KO) and parental B16F10 tumor growth following radiotherapy (10 Gy, single fraction, arrow) *in vivo*. $n = 10$ per group, ****, $P < 0.0001$, two-way ANOVA. **N,** ACSL3 knockout and parental B16F10 tumor growth following radiotherapy (8 Gy, single fraction, arrow) *in vivo*. $n = 10$ per group, ***, $P < 0.001$, two-way ANOVA. **O,** Relative lipid ROS levels in B16F10 cells treated with SAS (5 μmol/L), RSL-3 (0.05 μmol/L), or cyst(e)inase (10 μmol/L) and radiotherapy (2 Gy) *in vitro*. Representative biological triplicate shown, mean ± SD. ***, $P < 0.001$, two-way ANOVA. **P,** Tumor lipid ROS levels in B16F10 tumors following indicated radiotherapy dose fractionation *in vivo*. $n = 8$–10 per group, **, $P < 0.005$; ***, $P < 0.001$; ****, $P < 0.0001$, one-way ANOVA. Data are representative of at least two independent experiments (**A–P**).

we pretreated HT1080, B16F10, and ID8 cells with low doses of ferroptosis inducers (FIN) including sulfasalazine, RSL-3, erastin, and atorvastatin, and then irradiated these cells. We found that ferroptosis inducers reduced clonogenic cell survival as compared with radiotherapy alone in HT1080 cells *in vitro* (Fig. 1H). GPX4 utilizes glutathione to reduce oxidized lipid species and to limit ferroptosis. Glutathione levels are regulated by intracellular cystine concentrations. We depleted cystine and cysteine using cyst(e)inase, a recombinant human enzyme (18). Interestingly, cyst(e)inase strongly sensitized HT1080 cells to radiotherapy *in vitro* (Fig. 1I).

To support our finding in HT1080 cells, we treated B16F10 cells with sulfasalazine, RSL-3, and cyst(e)inase and observed decreased cell survival following radiotherapy as compared with radiotherapy alone (Supplementary Fig. S1J and S1K). Cell death quantification using propidium iodide (PI) staining confirmed that sulfasalazine and cyst(e)inase augmented radiation-induced cell death (Fig. 1J). Pretreatment with RSL-3, sulfasalazine, or cyst(e)inase also increased ID8 cell sensitivity to radiotherapy *in vitro* (Supplementary Fig. S1L and S1M). To examine the relevance of this finding *in vivo*, we established B16F10 tumors in C57BL/6 mice and treated mice with cyst(e)inase, radiotherapy, or the combination. Although cyst(e)inase had minimal efficacy as monotherapy, it enhanced radiotherapy efficiency (Fig. 1K). Moreover, increased tumor control was accompanied by enhanced lipid oxidation in the combination therapy group (Fig. 1L). Neither single treatment nor the combination treatment caused significant murine weight loss (Supplementary Fig. S1N).

To assess whether FINs can improve radiotherapy efficacy *in vivo*, we established B16F10 tumors in mice and treated tumors with radiotherapy, sulfasalazine, or both (dual treatment). We found that dual treatment enhanced tumor control (Supplementary Fig. S1O). Again, this improved tumoral control was accompanied by increased lipid oxidation in tumors treated with both agents (Supplementary Fig. S1P). These data suggest that ferroptosis can be targeted *in vivo* to enhance radiotherapy efficacy.

It has recently been shown that fatty-acid saturation modulates ferroptosis sensitivity. Specifically, ACSL4 promotes ferroptosis, whereas ACSL3 limits ferroptosis (19, 20). We generated ACSL4 knockout and ACSL3 knockout B16F10 cells (Supplementary Fig. S1Q and S1R). We observed that loss of the ferroptosis effector gene ACSL4 diminished radiotherapy efficacy *in vivo* (Fig. 1M). In contrast, deletion of the ferroptosis suppressor ACSL3 augmented radiotherapy efficacy *in vivo* (Fig. 1N).

To demonstrate that diminished cell survival following radiation was due to increased lipid peroxidation and ferroptosis, we quantified lipid peroxidation changes with C11BODIPY following FIN addition. We observed that in B16F10 cells, short exposures to low doses of sulfasalazine, RSL-3, and cyst(e)inase minimally altered lipid ROS. Combinations of FINs with radiation synergistically increased lipid ROS (Fig. 1O). FINs similarly augmented lipid ROS levels in concert with radiation in HT1080 cells (Supplementary Fig. S1S).

To generalize these findings to different radiation doses and fractionation schedules, we treated B16F10 tumors with 5 fractions of 3 Gy as well as a single fraction of 10 or 20 Gy. Quantification of lipid peroxidation changes with C11BODIPY showed that all radiotherapy doses induced increases in C11BODIPY, whereas higher single fractions of radiotherapy induced more lipid peroxidation (Fig. 1P). To confirm that ferroptosis resistance conferred radiotherapy resistance at ablative doses of radiotherapy, we treated wild-type (WT) and RSL-3–resistant B16F10 tumors with a single fraction of 20 Gy (21). We observed that even at higher doses of radiotherapy, ferroptosis-resistant tumors remained resistant to radiotherapy *in vivo* (Supplementary Fig. S1T).

Collectively, these data suggest that radiation induces tumor ferroptosis, and this ferroptosis can be pharmacologically augmented by ferroptosis agonists. Thus, targeting ferroptosis may be a novel therapeutic approach for radiation sensitization.

CD8$^+$ T Cells Promote Radiotherapy-Induced Ferroptosis via IFNγ

CD8$^+$ T cells are required for efficacy of ablative doses of radiotherapy *in vivo* (21, 22). The cellular and molecular bases for the interaction between T cells and radiotherapy are not fully defined. We first examined the involvement of CD8$^+$ T cells in radiation therapy efficacy in a B16F10 tumor–bearing mouse model at moderate clinically utilized radiation doses. We subcutaneously inoculated B16F10 cells into C57BL/6 mice and established tumors. Then, mice received a moderate dose of radiation (8 Gy) alone or with anti-CD8 mAb administration prior to radiotherapy. As expected, radiotherapy reduced tumor volume (Fig. 2A). However, CD8$^+$ T-cell depletion with anti-CD8 mAb treatment largely abolished radiotherapy-induced tumor reduction (Fig. 2A). This radiation dose induced tumor-cell ferroptosis (Supplementary Fig. S1B and S1H). To understand if CD8$^+$ T cells promoted ferroptosis in concert with radiotherapy, we treated B16F10 cells with naïve or activated T-cell supernatant. We found that exposure to a low dose of T-cell supernatant had minimal effect on B16F10 cell survival. Interestingly, T-cell supernatant synergized with radiotherapy to limit B16F10 clonogenic cell survival (Fig. 2B). Furthermore, T-cell supernatant and radiotherapy each independently enhanced lipid peroxidation in B16F10 cells, and their combination further augmented lipid peroxidation (Fig. 2C). Blockade of IFNγ signaling decreased T-cell supernatant-induced tumor STAT1 phosphorylation (Supplementary Fig. S2A) and diminished tumor lipid ROS production following combination treatment with T-cell supernatant and radiotherapy (Fig. 2C). These results suggest that CD8$^+$ T cells may promote tumor ferroptosis and induce radiosensitization via IFNγ.

To assess a direct link between IFNγ signaling and radiotherapy efficacy, we treated ID8 cells with IFNγ and radiotherapy and examined clonogenic cell survival. We observed that IFNγ and radiotherapy synergistically reduced clonogenic survival (Fig. 2D). We also observed diminished clonogenic cell survival following IFNγ and radiation treatment in B16F10 cells (Supplementary Fig. S2B). IFNγ and radiotherapy synergistically increased lipid ROS levels in ID8 cells (Fig. 2E), B16F10 cells (Supplementary Fig. S2C), and HT1080 cells (Supplementary Fig. S2D). To confirm that IFNγ increased radiation-induced cell death, we quantified PI$^+$ dying B16F10 cells following treatment with IFNγ,

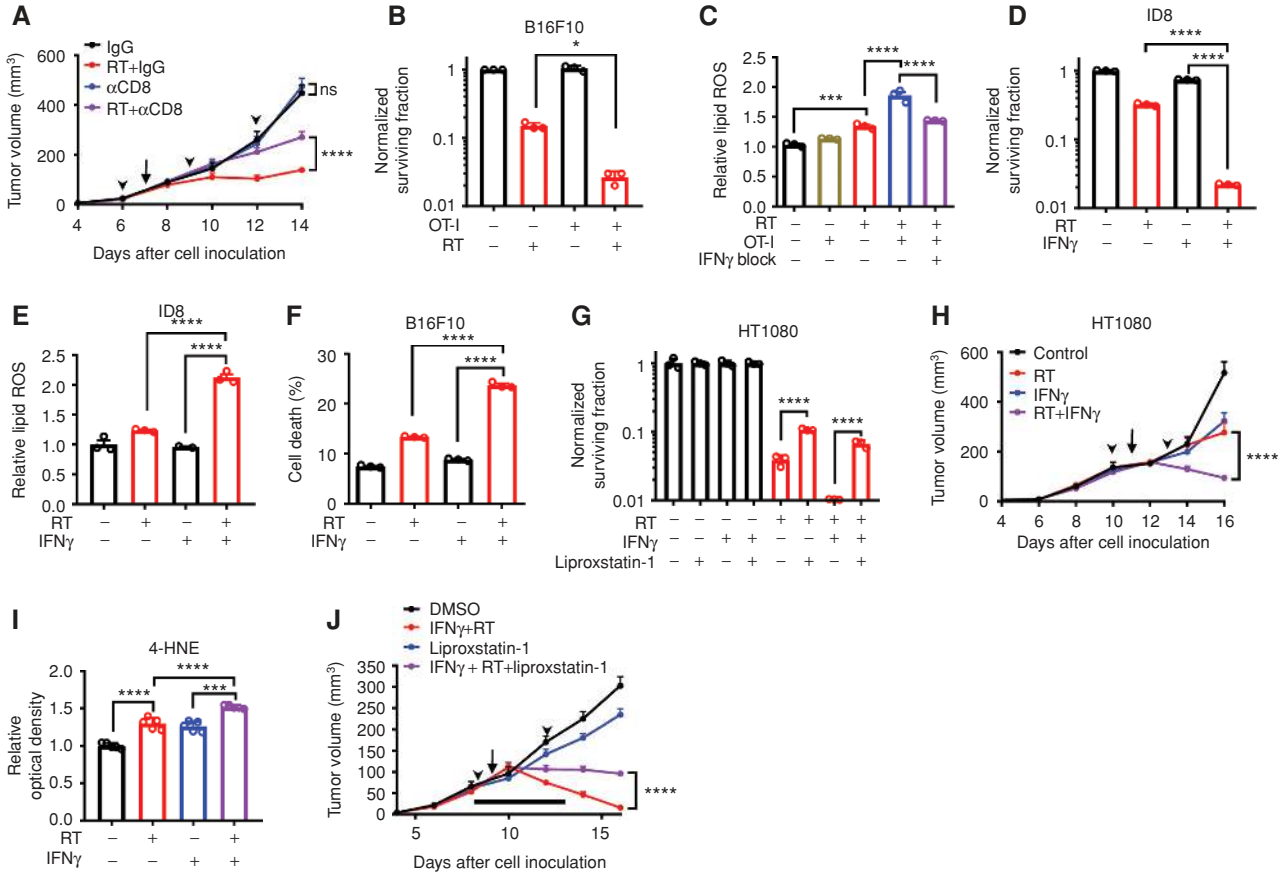

Figure 2. CD8⁺ T cells promote radiotherapy-induced ferroptosis via IFNγ. **A,** B16F10 tumor growth following irradiation (8 Gy, single fraction, arrow) and/or CD8⁺ T-cell depletion (arrowhead) *in vivo*. $n = 20$ per group, ****, $P < 0.0001$, two-way ANOVA. **B,** Clonogenic survival of B16F10 cells treated with naïve or activated (OT-I) CD8⁺ T-cell supernatant following RT (4 Gy) *in vitro*. Representative biological triplicate shown, mean ± SD. *, $P < 0.05$, one-way ANOVA. **C,** Relative lipid ROS levels of B16F10 cells treated with naïve or activated (OT-I) CD8⁺ T-cell supernatant following RT (4 Gy) with or without IFNγ signaling blockade *in vitro*. Representative biological triplicate shown, mean ± SD. ***, $P < 0.001$; ****, $P < 0.0001$, two-way ANOVA. **D,** Clonogenic survival of ID8 cells treated with IFNγ (10 ng/mL) and/or RT (4 Gy) *in vitro*. Representative biological triplicate shown, mean ± SD. ****, $P < 0.0001$, two-way ANOVA. **E,** ID8 cell relative lipid ROS levels following treatment with IFNγ and/or RT (4 Gy) *in vitro*. ****, $P < 0.0001$, two-way ANOVA. **F,** Cell death in B16F10 following treatment with IFNγ (10 ng/mL) and/or RT (20 Gy) *in vitro*. Representative biological triplicate shown, mean ± SD. ****, $P < 0.0001$, two-way ANOVA. **G,** Clonogenic survival of HT1080 cells following treatment with IFNγ (10 ng/mL), liproxstatin-1 (5 μmol/L), and/or RT (4 Gy) *in vitro*. Representative biological triplicate shown, mean ± SD. ****, $P < 0.0001$, two-way ANOVA. **H** and **I,** HT1080 tumor growth (**H**) and 4-HNE quantification (**I**) following treatment with RT (8 Gy, one fraction, arrow) and/or IFNγ (65 μg/mouse, intraperitoneal, arrowhead) *in vivo*. $n = 10$ per group. ***, $P < 0.001$; ***, $P < 0.0001$, two-way ANOVA. **J,** HT1080 tumor growth following treatment with liproxstatin-1 (intraperitoneal, 50 mg/kg, bar) and/or IFNγ (65 μg/mouse, arrowhead) and RT (6 Gy, arrow) *in vivo*. DMSO, $n = 10$; liproxstatin-1, $n = 11$; IFNγ+RT, $n = 15$; IFNγ+RT+liproxstatin-1, $n = 14$, ***, $P < 0.001$; ****, $P < 0.0001$, two-way ANOVA. Data are representative of at least two independent experiments (**A–J**).

radiotherapy, or the combination. We observed a synergistic increase in cell death following combination treatment with radiotherapy and IFNγ (Fig. 2F). To implicate ferroptosis in cell death induced by the combination treatment of radiotherapy and IFNγ, we conducted clonogenic survival experiments in HT1080 cells with IFNγ, radiotherapy, and liproxstatin-1. We observed that liproxstatin-1 administration blocked the synergistic reduction of cell survival observed upon treatment with IFNγ and radiotherapy (Fig. 2G; Supplementary Fig. S2E). The data indicate that the combination of IFNγ and radiotherapy regulates tumor-cell ferroptosis *in vitro*. To examine whether IFNγ alters radiotherapy efficacy *in vivo*, we inoculated HT1080 cells into NOD/SCID IL2γc-deficient (NSG) mice and treated mice with recombinant human IFNγ, radiotherapy, or the combination. Although low doses of IFNγ and radiotherapy slightly diminished tumor growth, the combination potently promoted tumor regression (Fig. 2H). To assess whether this is associated with tumor ferroptosis, we performed IHC staining in tumor tissues and quantified 4-hydoxynoneal (4-HNE), a lipid peroxidation by-product (23). Indeed, combination treatment with IFNγ and radiotherapy significantly increased tumoral 4-HNE levels (Fig. 2I; Supplementary Fig. S2F). To functionally demonstrate that ferroptosis contributed to synergistic tumor regression *in vivo*, we inoculated HT1080 cells into NSG mice and treated mice with IFNγ plus radiotherapy, liproxstatin-1, or all three agents. As expected, IFNγ plus radiotherapy induced tumor regression. Importantly, this effect was abrogated by simultaneous treatment with liproxstatin-1 (Fig. 2J). Together, these data demonstrate that CD8⁺ T cells directly sensitize tumor cells to radiotherapy through IFNγ by increasing lipid peroxidation and ferroptosis.

Radiotherapy and IFNγ Synergistically Suppress System SLC7A11

We next sought to define the molecular mechanism by which IFNγ sensitizes to radiotherapy and promotes tumor ferroptosis. We first performed unbiased RNA sequencing in HT1080 cells following treatment with IFNγ, radiotherapy, or the combination. Consistent with published results, interferon response genes, including *CXCL9* and *IRF1*, were upregulated strongly by IFNγ treatment (Fig. 3A; ref. 24). As expected, radiotherapy induced an ATM-dependent transcriptional program (25). Dual treatment with radiotherapy and IFNγ surprisingly downregulated multiple cystine and cysteine transport channels, including a component of the cystine–glutamate transporter system xc^-, SLC7A11 (Fig. 3A), which is a critical regulator of ferroptosis (26). Other ferroptosis regulators including GPX4, ACSL4, LPCAT3, and lipoxygenases (Supplementary Fig. S3A and S3B) were not altered in the same manner by dual treatment with radiotherapy plus IFNγ treatment. We next validated this finding. Treatment with IFNγ and radiotherapy individually reduced SLC7A11 transcripts (Fig. 3B) and protein levels (Fig. 3C) in HT1080 cells. Dual treatment resulted in a dramatic reduction of SLC7A11 in HT1080 cells (Fig. 3B and C). We also performed IHC staining for SLC7A11 in HT1080 tumor tissues (Fig. 2H) and found that IFNγ and radiotherapy reduced SLC7A11 expression *in vivo* (Fig. 3D). To determine the functional relevance of SLC7A11 reduction, we examined radiolabeled cystine uptake in HT1080 cells. Although both radiation and IFNγ each reduced cystine uptake, dual treatments resulted in a maximal decrease in cystine uptake in HT1080 cells (Fig. 3E). Cystine is a precursor for glutathione production, which is a required cofactor for GPX4 activity (27). To confirm that diminished cystine import altered cellular antioxidant stores, we quantified glutathione level in HT1080 cells following treatment with radiation, IFNγ, and the combination. We observed that the combination treatment significantly decreased glutathione level (Fig. 3F). Thus, radiotherapy and IFNγ synergistically downregulated SLC7A11 expression in tumor cells, resulting in diminished cystine transport and depletion of antioxidant stores in tumor cells to induce ferroptosis.

Next, we explored how radiotherapy downregulates SLC7A11 in tumor cells. Cells respond to radiotherapy through defined signaling cascades, including ATM activation (6, 25, 28). ATM has recently been shown to promote ferroptosis (29). We wondered whether ATM activation is involved in radiation-induced ferroptosis by regulating SLC7A11. To test this possibility, we treated HT1080 cells with KU60019 (30), an ATM inhibitor. ATM inhibition abrogated radiotherapy-mediated downregulation of SLC7A11 transcription (Supplementary Fig. S3C) and protein levels (Fig. 3G). Indeed, treatment with KU60019 diminished radiotherapy-induced lipid peroxidation in HT1080 cells (Fig. 3H). Further, siRNA targeting *ATM* prevented downregulation of SLC7A11 transcription (Supplementary Fig. S3D) and protein (Fig. 3I) following radiotherapy. To confirm this mechanism *in vivo*, we treated WT and sh*ATM* HT1080 tumors with radiotherapy (Supplementary Fig. S3E). We observed that WT but not ATM-silenced tumors showed downregulation of SLC7A11 expression (Fig. 3J; Supplementary Fig. S3F). Further, WT tumors showed increased 4-HNE lipid peroxidation *in vivo* following radiotherapy as compared with ATM-silenced tumors (Supplementary Fig. S3G and S3H). Therefore, radiotherapy transcriptionally represses SLC7A11 expression via ATM to promote tumoral ferroptosis.

We have previously reported that IFNγ negatively regulates SLC7A11 expression in a JAK–STAT1-dependent manner (16, 31). To validate this finding, we silenced STAT1 with siRNAs (si*STAT1*) in HT1080 cells and found that IFNγ downregulated SLC7A11 in a STAT1-dependent manner (Supplementary Fig. S3I; Fig. 3K). Interestingly, IFNγ efficiently and comparably reduced SLC7A11 expression in both ATM-proficient and ATM-deficient HT1080 cells (Supplementary Fig. S3J). Conversely, regardless of STAT1 expression, radiotherapy efficiently reduced SLC7A11 expression in HT1080 cells (Supplementary Fig. S3K). Thus, radiotherapy and IFNγ synergistically repress tumor SLC7A11 through ATM and STAT1 signaling, respectively. To confirm this mechanism *in vivo*, we treated WT and STAT1 knockout HT1080 tumors with IFNγ (Supplementary Fig. S3L). We observed that WT but not STAT1-deficient tumors showed SLC7A11 downregulation following IFNγ treatment (Fig. 3L; Supplementary Fig. S3M). We also observed that WT tumors showed increased 4-HNE lipid oxidation following IFNγ treatment as compared with STAT1 knockout tumors (Supplementary Fig. S3N and S3O).

To functionally connect SLC7A11 to tumor ferroptosis induced by radiotherapy, we used small hairpin RNAs against SLC7A11 (sh*SLC7A11*) to knock down SLC7A11 in HT1080 cells (Supplementary Fig. S3P). We found that knockdown of SLC7A11 promoted radiotherapy-induced cell death in HT1080 cells (Fig. 3M) and B16F10 cells (Supplementary Fig. S3Q). This effect was rescued by liproxstatin-1 in HT1080 cells (Fig. 3M) and B16F10 cells (Supplementary Fig. S3Q). To determine the importance of SLC7A11 in radiotherapy *in vivo*, we used CRISPR/Cas9 to delete SLC7A11 in B16F10 cells. We confirmed deletion by quantifying *SLC7A11* mRNA levels, and, consistent with loss of system xc^- function, knockout cells were unable to export glutamate (Supplementary Fig. S3R and S3S). In line with previous reports (12, 26), we found SLC7A11-deficient cells underwent spontaneous cell death, which can be rescued by liproxstatin-1 or 2-mercaptoethanol (Supplementary Fig. S3T). We inoculated SLC7A11-proficient and SLC7A11-deficient B16F10 tumors into C57BL/6 mice and treated mice with radiotherapy. Radiotherapy efficacy was enhanced in SLC7A11-deficient cells *in vivo* (Fig. 3N). Examination of lipid peroxidation showed that SLC7A11-deficient tumors had increased baseline levels of lipid ROS (Fig. 3O). Moreover, radiotherapy-induced alterations in lipid peroxidation were further increased by loss of SLC7A11 (Fig. 3O). To confirm the importance of SLC7A11 to survival following combination IFNγ and radiotherapy, we overexpressed SLC7A11 in HT1080 cells (Supplementary Fig. S3U). We observed that overexpression significantly increased clonogenic survival following treatment with radiotherapy and IFNγ (Fig. 3P). To further confirm the importance of SLC7A11 expression, we performed rescue experiments in which SLC7A11 was expressed in SLC7A11-deficient cells (Supplementary Fig. S3V). In addition, we observed that overexpression of SLC7A11 reversed

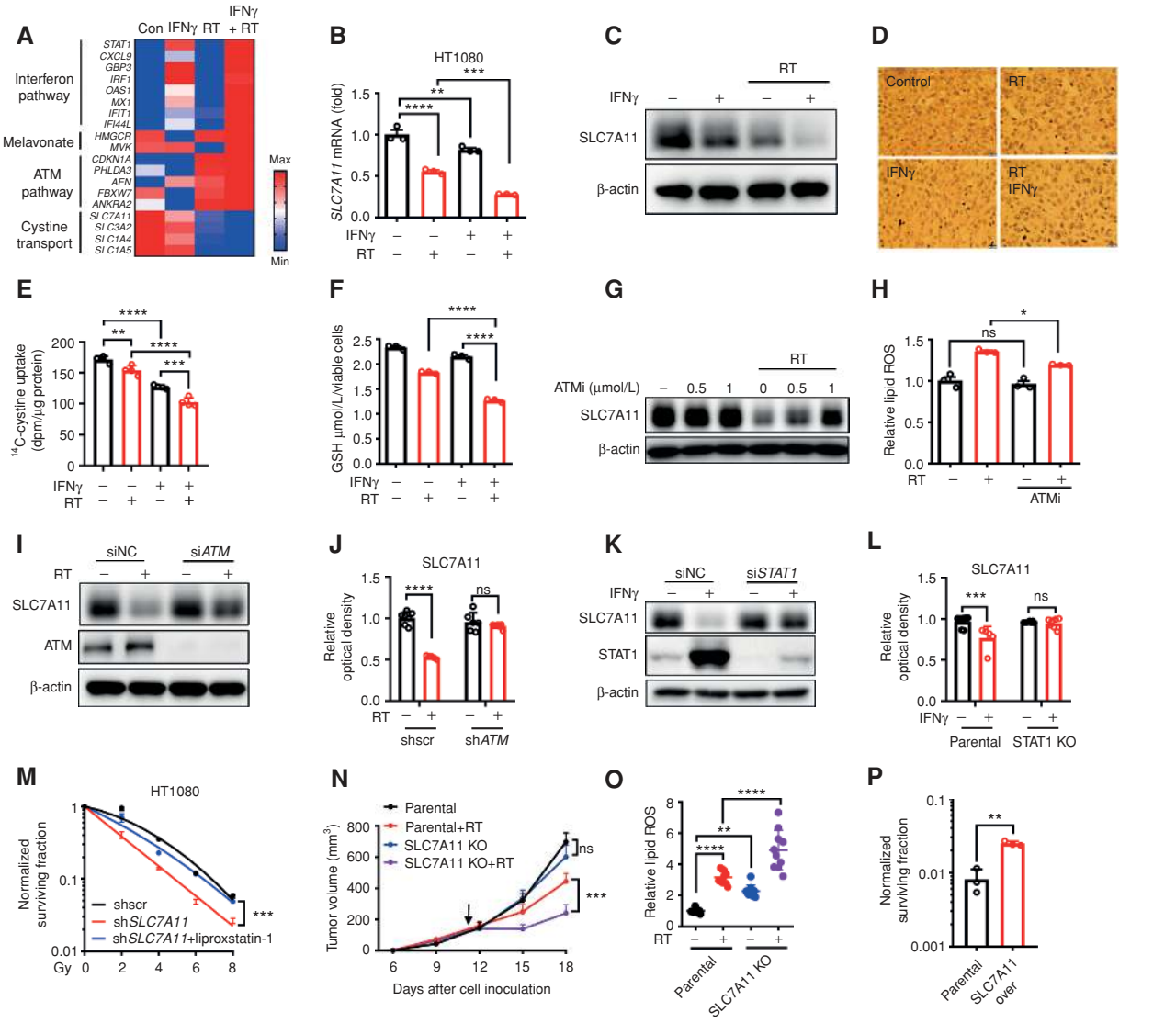

Figure 3. Radiotherapy and IFNγ synergistically suppress system SLC7A11. **A,** Normalized heat map of HT1080 RNA sequencing following treatment with IFNγ (10 ng/mL) and/or RT (20 Gy) *in vitro*. **B,** qPCR for SLC7A11 in HT1080 cells treated with IFNγ (10 ng/mL) and/or RT (10 Gy) *in vitro*. **, $P < 0.01$; ***, $P < 0.001$; ****, $P < 0.0001$, two-way ANOVA. **C,** Immunoblot for SLC7A11 in HT1080 cells treated with IFNγ (10 ng/mL) and/or RT (10 Gy) *in vitro*. **D,** Representative SLC7A11 IHC in HT1080 tumors treated as in Fig. 2H *in vivo*. **E,** ^{14}C-cystine uptake in HT1080 cells treated with IFNγ (10 ng/mL) and/or RT (10 Gy) *in vitro*. **, $P < 0.01$; ***, $P < 0.001$; ****, $P < 0.0001$, two-way ANOVA. **F,** Glutathione quantification in HT1080 cells treated with IFNγ (10 ng/mL) and/or RT (16 Gy) *in vitro*. ****, $P < 0.0001$, two-way ANOVA. **G,** Immunoblot in HT1080 cells irradiated with RT (10 Gy) and/or KU60019 *in vitro*. **H,** HT1080 lipid ROS following RT (4 Gy) and/or KU60019 (1 μmol/L) *in vitro*. Representative biological triplicate shown, mean ± SD. ns, $P > 0.05$; *, $P < 0.05$, two-way ANOVA. **I,** Immunoblot for indicated protein in HT1080 cells treated with 10 Gy (RT) and/or siRNA targeting ATM (si*ATM*) *in vitro*. **J,** IHC quantification of SLC7A11 in HT1080 tumors of the indicated genotypes following treatment with RT (8 Gy, single fraction, arrow) *in vivo*. ns, $P > 0.05$; ****, $P < 0.0001$, two-way ANOVA. **K,** Immunoblot for indicated protein in HT1080 cells treated with IFNγ (10 ng/mL) and/or siRNA targeting STAT1 (si*STAT1*) *in vitro*. **L,** IHC quantification of SLC7A11 in HT1080 tumors, treated with or without IFNγ (65 μg/mouse, intraperitoneal). ns, $P > 0.05$; ****, $P < 0.0001$, two-way ANOVA. **M,** Clonogenic survival of HT1080 cells at indicated RT dose following shRNA targeting SLC7A11 (sh*SLC7A11*) and liproxstatin-1 treatment *in vitro*. Representative biological triplicate shown, mean ± SD. ***, $P < 0.001$, one-way ANOVA. **N** and **O,** SLC7A11 knockout B16F10 cells tumor growth (**N**) and tumor lipid ROS levels (**O**) following irradiation (8 Gy, single fraction, arrow) *in vivo*. Parental, $n = 15$; Parental+RT, $n = 19$; SLC7A11 KO, $n = 17$; SLC7A11 KO+RT, $n = 18$. **N,** ***, $P < 0.001$, two-way ANOVA; **O,** **, $P < 0.01$; ****, $P < 0.0001$, two-way ANOVA. **P,** Clonogenic survival of WT and SLC7A11-overexpressing (SLC7A11 over) HT1080 cells following 8 Gy and IFNγ (10 ng/mL) *in vitro*. **, $P < 0.001$, unpaired Student *t* test. **Q,** SLC7A11 knockout with/without SLC7A11 overexpression B16F10 cells tumor growth following irradiation (8 Gy, single fraction, arrow) *in vivo*. $n = 10$, *, $P < 0.05$; ****, $P < 0.0001$, two-way ANOVA. Data are representative of at least two independent experiments (**A–Q**).

the sensitivity of SLC7A11-deficient tumors to radiotherapy *in vivo* (Fig. 3Q). Collectively, these results suggest that radiotherapy-activated ATM and IFNγ-induced STAT1 signaling jointly target SLC7A11 to modulate cystine uptake and promote tumor lipid peroxidation and ferroptosis.

Radiotherapy and Immunotherapy Synergistically Induce Tumoral Ferroptosis

Immunotherapy augments radiotherapy efficacy *in vivo*, but the mechanisms through which immune checkpoint blockade enhances tumor-cell death in irradiated lesions are not well defined (4, 32, 33). Checkpoint therapy including anti–PD-L1 and anti-CTLA4 activates $CD8^+$ T cells and potentiates the IFNγ signaling pathway to control tumor progression (1). We hypothesized that radiotherapy and immunotherapy would synergize via ferroptosis *in vivo* to improve the efficacy of both therapies. To test this hypothesis, we established B16F10 tumors in C57BL/6 mice and treated mice with anti-CTLA4 mAb, radiotherapy, or the combination. As previously reported, anti-CTLA4 monotherapy was minimally efficacious in B16F10 tumors (32). However, we found that it potentiated radiotherapy efficacy in irradiated tumors (Fig. 4A). Consistent with our observations (Fig. 1), radiotherapy increased lipid peroxidation. Interestingly, the combination treatment with anti-CTLA4 and radiotherapy further enhanced tumoral lipid peroxidation (Fig. 4B). The combination of anti-CTLA4 and radiotherapy enhanced $CD8^+$ T-cell trafficking into tumors (Supplementary Fig. S4A and S4B). Radiotherapy increased tumor-infiltrating $Ki67^+CD8^+$ T cells, and this was augmented by anti-CTLA4 (Fig. 4C; Supplementary Fig. S4C). Furthermore, we detected enhanced $CD8^+$ T-cell function following combined anti-CTLA4 and radiotherapy as marked by increased IFNγ and granzyme B production (Fig. 4D and E; Supplementary Fig. S4D and S4E). Similarly, we observed that combination therapy increased $CD4^+$ T-cell number and IFNγ expression (Supplementary Fig. S4F and S4G). To determine whether tumor ferroptosis contributed to the synergy between anti-CTLA4 and radiotherapy *in vivo*, we inoculated B16F10 tumors in C57BL/6 mice and treated them with the combination of anti-CTLA4 plus radiotherapy, liproxstatin-1, or all three treatments. Interestingly, liproxstatin-1 diminished the combined therapeutic efficacy of anti-CTLA4 and radiotherapy as shown by tumor volume (Fig. 4F), as well as tumor lipid peroxidation (Supplementary Fig. S4H). To extend our findings to an additional model, we inoculated ID8 tumors into the peritoneal cavities of C57BL/6 mice, and treated mice with anti-CTLA4, radiotherapy, or the combination. Anti-CTLA4 and radiotherapy synergistically enhanced tumor control *in vivo* (Fig. 4G). Again, we observed increased lipid peroxidation following radiotherapy, and anti-CTLA4 mediated enhancement of lipid peroxidation following dual treatment with radiotherapy and anti-CTLA4 (Fig. 4H). To explore if other forms of immune checkpoint blockade also induced lipid peroxidation, we established B16F10 tumors in mice and treated the tumors with radiotherapy, anti–PD-L1, or both. Although anti–PD-L1 or radiotherapy alone controlled tumor growth, the dual treatment was more effective in reducing tumor growth than any single therapy (Fig. 4I). We also detected the highest levels of tumor lipid peroxidation following combination therapy (Fig. 4J).

SLC7A11-deficient cells were more sensitive to radiotherapy *in vitro* and *in vivo* because of their increased ferroptosis susceptibility (Fig. 3). We hypothesized that ferroptosis-sensitive tumors may benefit more from immune checkpoint blockade. To examine this, we established SLC7A11-proficient or SLC7A11-deficient B16F10 tumors in C57BL/6 mice and treated mice with anti–PD-L1. We detected higher tumoral lipid ROS in SLC7A11-deficient tumor cells than in WT tumor cells regardless of anti–PD-L1 therapy (Supplementary Fig. S4I). Furthermore, SLC7A11-deficient tumors were more sensitive to anti–PD-L1 therapy, as shown by increased tumor C11BODIPY fluorescence and reduced tumor volume (Supplementary Fig. S4J) compared with WT tumors.

To additionally support that ferroptosis is a mechanism of synergy between immunotherapy and radiotherapy, we inoculated parental or RSL-3 ferroptosis-resistant cells into mice and treated mice with anti–PD-L1 and radiotherapy. We observed that in contrast to the parental cells, RSL-3–resistant B16F10 cells were largely insensitive to combined treatment with anti–PD-L1 and radiotherapy (Fig. 4K). Moreover, this insensitivity was accompanied by diminished C11BODIPY in tumor cells (Fig. 4L). To define the mechanisms contributing to resistance to therapy, we established ovalbumin expressing parental or RSL-3 ferroptosis-resistant B16F10 tumors and treated the mice with OT-1 transgenic T cells. We observed that OT-1 therapy controlled WT but not RSL-3–resistant tumors. This suggests that ferroptosis-resistant tumors are resistant to T-cell effector function (Fig. 4M).

To examine whether SLC7A11 modulated the induction of durable immune responses, we established parental or SLC7A11-deficient B16F10 tumors and treated them with radiotherapy and anti–PD-L1 therapy. We observed that SLC7A11-deficient tumors were more sensitive to combination therapy, with complete long-term responses in 56% (14/25) of SLC7A11-deficient tumor-inoculated mice (Fig. 4N). To test whether these mice developed immunologic memory, WT B16F10 tumors were reinoculated in cured mice. We noted that tumors established in control but not previously cured mice, suggestive of the establishment of T-cell memory (Fig. 4O). Collectively, these data suggest that immunotherapy synergizes with radiotherapy to induce tumor ferroptosis and establish T-cell immunity.

DISCUSSION

A major challenge in oncology is how to rationally and effectively integrate PD-1/PD-L1 and CTLA4 immune checkpoint blockade with traditional oncologic treatment modalities, including radiotherapy (1). $CD8^+$ T cells are required for the efficacy of both immunotherapy and radiotherapy. We have now demonstrated that effector T cells and radiotherapy interact through ferroptosis to promote tumor clearance. Radiotherapy classically promotes tumor-cell death primarily through the induction of double-stranded DNA breaks in tumor cells which, if unrepaired, lead to mitotic catastrophe and unregulated tumor cell death (7). We provide the first evidence that radiation also promotes lipid peroxidation, resulting in tumoral ferroptosis. Concurrent administration of genotoxic agents to augment DNA damage has been harnessed clinically to improve radiotherapy efficacy and improve the outcomes of patients with

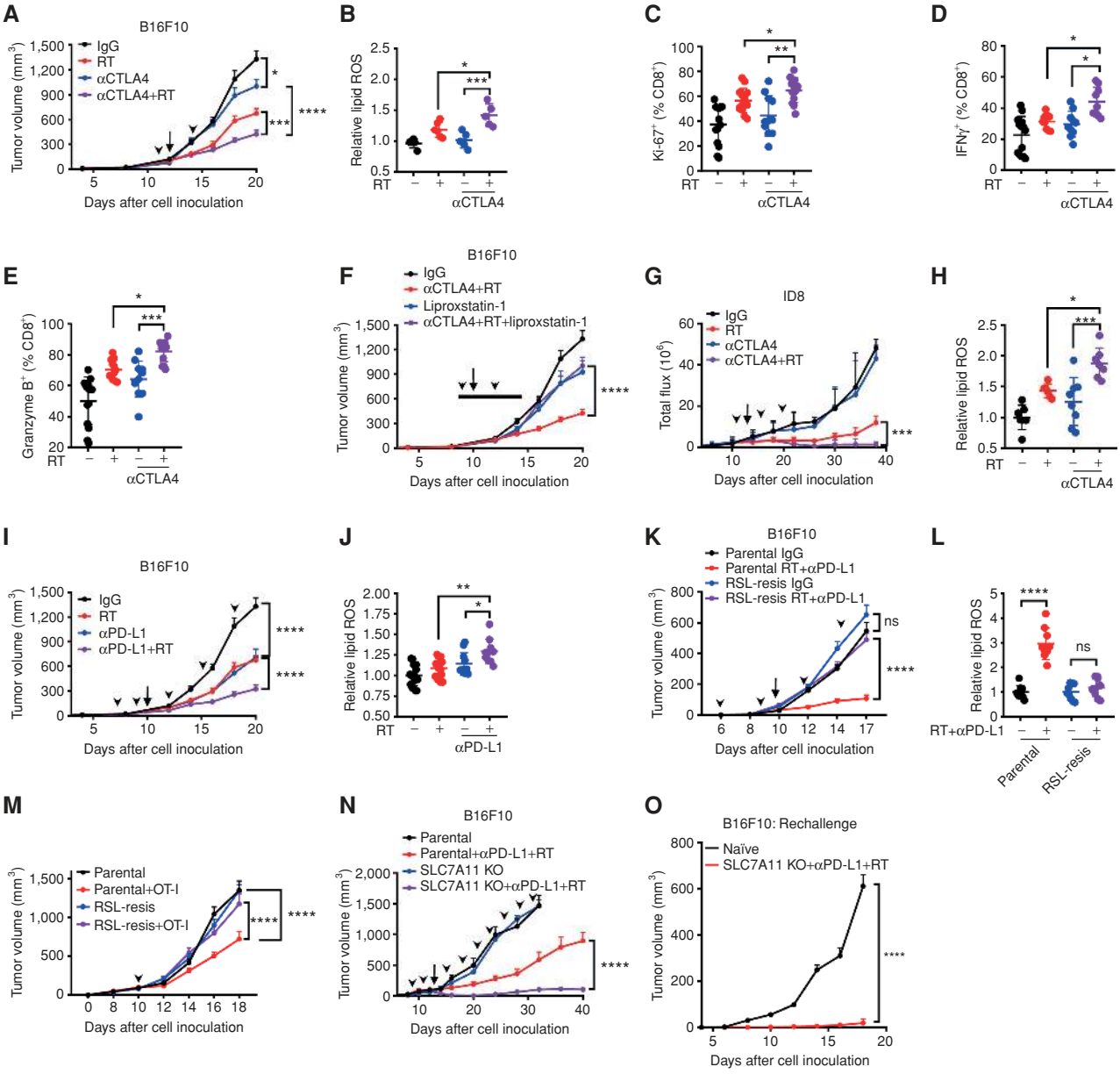

Figure 4. Radiotherapy and immunotherapy synergistically induce tumoral ferroptosis. **A** and **B,** B16F10 (**A**) tumor growth and (**B**) tumor lipid ROS levels following treatment with RT (8 Gy) and/or anti-CTLA4 mAb *in vivo*. Isotype control (IgG), $n = 16$; RT, $n = 20$; anti-CTLA4 mAb (αCTLA4), $n = 18$; RT+αCTLA4 mAb (αCTLA4+RT), $n = 20$, **A,** *, $P < 0.05$; ***, $P < 0.001$; ****, $P < 0.0001$, two-way ANOVA; **B,** *, $P < 0.05$; ***, $P < 0.001$, two-way ANOVA. **C,** Intratumoral CD8+ T-cell proliferation *in vivo*. *, $P < 0.05$; **, $P < 0.01$, two-way ANOVA. **D,** IFNγ production by intratumoral CD8+ T cells *in vivo*. *, $P < 0.05$, two-way ANOVA. **E,** Granzyme B production by intratumoral CD8+ T cells *in vivo*. *, $P < 0.05$; ***, $P < 0.001$, two-way ANOVA. **F,** B16F10 tumor growth following treatment with liproxstatin-1 (50 mg/kg, intraperitoneal, bar) and/or RT (8 Gy, single dose, arrow) with anti-CTLA4 mAb (arrowhead) *in vivo*. Isotype control (IgG), $n = 16$; RT, $n = 20$; liproxstatin-1, $n = 8$; RT plus anti-CTLA4 mAb and liproxstatin-1 (αCTLA4+RT+liproxstatin-1), $n = 20$, ****, $P < 0.0001$, two-way ANOVA. **G** and **H,** ID8 (**G**) tumor growth and (**H**) lipid ROS following treatment with RT (8 Gy, single dose, arrow) and/or anti-CTLA4 mAb (arrowhead) *in vivo*. $n = 8$ per group, *, $P < 0.01$; ***, $P < 0.001$, two-way ANOVA. **I** and **J,** B16F10 tumor cell growth (**I**) and tumor lipid ROS levels (**J**) following treatment with RT (8 Gy, single dose, arrow) and/or anti-PD-L1 mAb (200 μg/mouse, arrowhead) *in vivo*. Isotype control (IgG), $n = 15$; RT, $n = 16$, anti-PD-L1 mAb (αPD-L1); $n = 17$, RT and anti-PD-L1 mAb (αPD-L1+RT), $n = 17$. **I,** ****, $P < 0.0001$, two-way ANOVA; **J,** *, $P < 0.05$; **, $P < 0.01$, two-way ANOVA. **K** and **L,** RSL-3–resistant B16F10 tumor growth *in vivo* (**K**) and tumoral lipid ROS (**L**) were treated with RT (8 Gy, one fraction, arrow) and anti-PD-L1 mAb (200 μg/mouse, arrowhead). Parental IgG, $n = 14$; parental RT+αPD-L1, $n = 16$; RSL-resis IgG, $n = 14$; RSL-resis RT+αPD-L1, $n = 16$. **K,** ns, $P > 0.05$; ****, $P < 0.0001$, two-way ANOVA; **L,** ns, $P > 0.05$; ****, $P < 0.0001$, two-way ANOVA. **M,** RSL-3–resistant or parental ovalbumin-expressing B16F10 tumor growth following adoptive transfer of activated OT-I T cells *in vivo* (arrowhead). $n = 10$, ****, $P < 0.0001$, two-way ANOVA. **N** and **O,** SLC7A11 knockout B16F10 tumor growth (**N**) and rechallenge inoculation (**O**) following irradiation (8 Gy, single fraction, arrow) and anti-PD-L1 treatment (200 μg/mouse, arrowhead) *in vivo*. Parental, $n = 10$; parental+αPD-L1+RT, $n = 10$; SLC7A11 KO, $n = 10$; SLC7A11 KO+αPD-L1+RT, $n = 25$; naïve, $n = 10$. ****, $P < 0.0001$, two-way ANOVA. Data are representative of at least two independent experiments (**A–O**).

cancer. We have found that ferroptosis agonists can sensitize tumors to radiation both *in vitro* and *in vivo,* uncovering new therapeutic strategies to improve radiotherapy efficacy.

Ferroptosis is regulated by lipid metabolism, iron metabolism, and cysteine metabolism (34). ATM regulates cell survival following radiotherapy (25) and has also been shown to regulate ferroptosis (29). We have shown that radiotherapy activates ATM to suppress SLC7A11 expression, limit tumor cystine uptake, and diminish glutathione, and increases lipid oxidative damage to mediate tumor-cell ferroptosis. We have demonstrated that biochemical and genetic inhibition of ATM can prevent loss of SLC7A11 expression, reduce lipid oxidation, and rescue tumor-cell ferroptosis induced by radiotherapy. Similarly, ATM promotes DNA-damage repair and cell survival following radiation but is also required for radiation-induced ferroptosis. Along this line, p53 contributes to tumor-cell survival but also promotes tumor-cell death (35). Several pharmacologic inhibitors are being studied as radiosensitizers (36). Given that ATM signaling may play an unexpected role in promoting tumor-cell ferroptosis, additional study is required to understand the context-dependent consequence of ATM inhibition. Notably, we have focused on a role of SLC7A11 and ATM in radiotherapy-associated ferroptosis. We do not rule out that radiation may affect other ferroptosis-associated genes, which may collectively contribute to radiotherapy-mediated ferroptosis in different contexts.

$CD8^+$ T-cell tumor infiltration and IFNγ signaling pathway activation are key features of effective immunotherapy in patients with cancer (1, 37, 38). We have recently shown that $CD8^+$ T cells modulate tumoral ferroptosis (16). We now extend this work, showing that $CD8^+$ T cells can alter the sensitivity of tumor cells to radiotherapy by promoting ferroptosis. $CD8^+$ T cell–derived IFNγ and radiation coordinately inhibit tumor SLC7A11 expression to induce tumor-cell ferroptosis. This translates into potent tumor immunity, tumor ferroptosis, and tumor regression in several murine models treated with the combination of radiotherapy and PD-L1/PD-1 or CTLA4 blockade. Moreover, ferroptosis inhibition or resistance diminishes the synergy between immunotherapy and radiotherapy *in vivo*. The major immunosuppressive mechanisms in the tumor microenvironment include high PD-L1 expression (39, 40) and regulatory T-cell infiltration (41). Radiation can target PD-L1–expressing cells and regulatory T cells (15). More recently, cGAS–STING sensing of cytoplasmic DNA and micronuclei following radiation has emerged as an important connection between innate immunity and radiotherapy (3, 4, 32). Our work suggests that tumor ferroptosis is a novel intersection between radiotherapy and adaptive immunity.

In conclusion, this work highlights that ferroptosis may be an untapped therapeutic mechanism and focus for the development of effective pharmacologic and immunotherapeutic combinatorial approaches with radiotherapy for the treatment of cancer.

METHODS

Reagents

Ferrostatin-1 (347174-05-4), liproxstatin-1 (950455-15-9), trolox (53188-07-1), DFO (138-14-7), RSL-3 (1219810-16-8), erastin (571203-78-6), sulfasalazine (599-79-1), atorvastatin (599-79-1), and KU60019 (925701-46-8) were purchased from Cayman. The concentration used is shown in Supplementary Table. S1. C11BODIPY (D3861) was purchased from Invitrogen. Mouse recombinant IFNγ (485-MI-100), anti-mouse IFNγ block antibody (MAB485), and human recombinant IFNγ (285-IF-100) were purchased from R&D. Anti-mouse IFNGR1 antibody (16-1193-85) was purchased from Thermo Fisher. The following antibodies were used for immunoblots: Anti-human SLC7A11 antibody (12691), anti-β-actin (12262), anti-GAPDH (2118), anti-STAT1 (9172), anti–phospho-STAT1 (9167), anti-ATM (2873), and anti-ACSL4 (4047) were bought from Cell Signaling Technology. Anti-GPX4 (ab41787) was from Abcam. In addition, IgG (BE0087, BE0090), anti-mouse CTLA4 (BE0131), anti-mouse PD-L1 (BE0101), and anti-mouse CD8 (BE0117) were purchased from BioXcell. 4-HNE antibody (ab46545) was purchased from Abcam. Cyst(e)inase was generated as previously described (18).

Cell Lines

All the cell lines used here, including B16F10, ID8, HT1080, and HEK-293T cell lines, were bought from the ATCC. Cells were regularly tested for *Mycoplasma* contamination using the Adenosine 5′-triphosphate (ATP) Bioluminescent Assay Kit (Sigma) every 2 weeks. Cells were thawed at early passage and cultured for up to 16 weeks in total.

Flow Cytometry

To assess cell death, cells were treated as indicated, then collected and stained with PI. For *in vitro* C11BODIPY analysis, cells were treated with test compounds for the indicated times, then harvested and incubated with C11BODIPY (581/591) for 20 minutes at 37°C. For *ex vivo* C11BODIPY analysis, tumors were filtered and underwent gradient centrifugation, then were incubated with 2 μmol/L C11BODIPY and anti-CD45 antibody. C11BODIPY FITC channel median fluorescence intensity data were normalized to untreated controls. To quantify T-cell cytokine production, mononuclear cells were isolated, stained, and analyzed as previously described (40).

Radiotherapy

Radiotherapy was delivered using a Philips RT250 model orthovoltage unit (Kimtron Medical) or a Small Animal Radiation Research Platform (XStrahl Medical and Life Sciences) at a dose rate of approximately 2 Gy per minute as previously described (42). Experiments were performed in the Experimental Irradiation Shared Resource (University of Michigan). Focal irradiation was provided to flank tumors via lead shielding or collimation. Whole-abdominal radiotherapy was provided to intraperitoneal tumors with shield above the diaphragm and below the pelvis.

Clonogenic Survival Assay

Clonogenic survival analysis was conducted as previously described. Normalized surviving fraction was represented as relative to compound alone as previously described (42).

Animal Studies

Six- to 8-week-old NSG and WT C57BL/6 mice were obtained from the Jackson Laboratory. OT-I colony was maintained internally. All mice were maintained under specific pathogen–free housing with a maximum of 5 mice per cage. Mice were randomized to experimental groups when tumors reached 50 mm^3 (HT1080, B16F10) or on day of first bioluminescent imaging (ID8). Tumor size was quantified, and anti–PD-L1 was provided as previously described (16). For IFN experiments, 65 μg of human IFNγ was given 24 hours prior to radiation (6–8 Gy, single fraction) as well as 2 days after radiotherapy. The primary endpoint of all experiments was tumor size. All the animal studies were conducted under the approval of the University of Michigan Committee on Use and Care of Animals (PRO00008278).

Activated T-cell Supernatant Harvest

Single-cell suspension was prepared from spleens and lymph nodes from OT-I mice, then stimulated with 5 μg/mL OVA peptide (Sigma, S7951) in RPMI-1640 medium containing 10% FBS. After 3 days, $CD8^+$ T cells were isolated via magnetically labeled antibodies (StemCell Technologies, 19853) and then cultured in RPMI-1640 medium containing IL2 (R&D Biosystems) and 2-mercaptoethanol (Gibco, 21985023). After 3 days, supernatant was harvested and filtered through 0.2-μm filter prior to subsequent use. For blocking, B16F10 cells were pretreated with 10 μg/mL anti-IFNGR as well as 10 ng/mL anti-IFNγ antibody.

Immunohistochemistry

Tumor tissues were harvested and fixed in 10% formalin and embedded in paraffin. Staining was performed on tumors treated with the indicated conditions using anti–4-HNE or anti-SLC7A11 antibody and counterstained using hematoxylin. The alkaline phosphatase optical density was quantified in ImageJ. Results were normalized to untreated controls.

RNA Sequencing

Cell lines were treated as indicated, and total RNA was purified using an mRNA kit (Qiagen). Libraries were prepared as previously described, and the edgeR package was used to generate reads per kilobase of transcript per million mapped reads values (43). Differential expression analysis was performed using the limma-R package as previously described. Minmax data normalization was used for heat-map generation. Gene set enrichment analysis was performed to identify significantly enriched gene sets (FDR < 0.20). Gene Expression Omnibus accession number: GSE137946.

Real-Time PCR

Total RNA was extracted using TRIzol and phenol-chloroform phase separation. Reverse transcription was performed using the RevertAid RT Reverse Transcription Kit (Invitrogen, K1691). SYBR Green (Invitrogen, 4368702) was used for quantitative PCR with a StepOne Real Time PCR system (Applied Biosystems). β-actin was used as an internal control. Results are represented as fold change from untreated controls. The sequences of primers for qPCR are as follows:

Human SLC7A11 forward: 5′-TGCTGGGCTGATTTTATCTTCG-3′,
Human SLC7A11 reverse: 5′-GAAAGGGCAACCATGAAGAGG-3′,
Human β-actin forward: 5′-TGGTATCGTGGAAGGACTC-3′,
Human β-actin reverse: 5′-AGTAGAGGCAGGGATGATG-3′,
mouse ACSL3 forward: 5′-TCCTGGCTGCGATACACTTG-3′,
mouse ACSL3 reverse: 5′- CCAAAGTCAAGGGCTCGGAT-3′,
mouse β-actin forward: 5′-TGAGCTGCGTTTTACACCCT-3′,
mouse β-actin reverse: 5′-TTTGGGGGATGTTTGCTCCA-3′

Generation of Genetically Modified Cell Lines

HEK-293T cells were transfected with a nontargeted retroviral vector, or a retroviral vector encoding shRNA targeting SLC7A11. Virus-containing supernatant was harvested, and HT1080 cells and B16F10 cells were transduced and selected prior to subsequent use.

Dharmacon shRNA sequence:

Human sh*SLC7A11*: ATAATAAAGAGATAATACG
Mouse sh*SLC7A11*: ATTAGCTGTATAACTCCAGGG

CRISPR/Cas9 constructs (Santa Cruz Biotechnology) were utilized to generate B16F10 subclones deficient in ACSL4 (sc-424503-NIC) and SLC7A11 (sc-424104-NIC). In addition, 2-mercaptoethanol (Gibco, 21985023) was added to support SLC7A11 knockout cell growth. lentiCRISPR v2 (Addgene, 52961)-based constructs were used for knockout of ACSL3 in B16F10 cells, and the designed gRNA sequences were GTAATGATATGCCGCAGACG and GGTGTG TACAATGACACCTT. HEK-293T cells were used to produce lentivirus. B16F10 cells were infected with scramble control or gene-targeted lentivirus and selected with 2 μg/mL puromycin prior to subsequent use.

To perform the ectopic SLC7A11 rescue assay, a cytomegalovirus promoter-driven mouse SLC7A11-IRES-GFP construct was generated by Gibson Assembly. This construct was transfected into SLC7A11-deficient B16F10 cells. Clones were selected with G418 and fluorescence-activated cell sorting.

RNA Interference (siRNA)

HT1080 cells were transfected with control or siRNA targeting human ATM (4392420-S532284, Thermo Fisher) or STAT1 (SASI_Rn02_00204016, Sigma) using lipofectamine RNAiMAX (Invitrogen) prior to experimentation.

Radiolabeled Cystine Uptake Assay

HT1080 cells were treated with either IFNγ (10 ng/mL), radiotherapy (10 Gy), or both for 24 hours. Medium was removed and changed to cystine-free medium. L-^{14}C-Cystine (0.2 μCi/mL) was added and incubated for 15 to 45 minutes. Cells were washed and lysed. A Beckman liquid scintillation counter was used to quantify radioactive cystine uptake. Results were normalized to total protein as determined by Pierce BCA Protein Assay Kit (Thermo, 23225).

Glutathione Assay

HT1080 cells were treated with either IFNγ (10 ng/mL), radiotherapy (16 Gy), or both for 24 hours. Glutathione was quantified using the GSH-Glo assay (Promega). Results were normalized to cell viability.

Glutamate Assay

The Glutamate Colorimetric Assay Kit (BioVision, K629) was used for detection of extracellular glutamate released into the medium. Parental or SLC7A11 knockout B16F10 cells were seeded overnight in the presence of 2-mercaptoethanol to support knockout cell growth. Results normalized to cell viability.

Cell Viability Assay

Cells were collected and seeded into 96-well plates. To determine the effect of treatment on cell growth and viability, 10% volume of alamarBlue (Bio-Rad) was added directly into the medium and incubated for 4 hours. Absorbance at wavelengths of 570 and 600 nm was measured. Results were normalized to untreated controls and shown as relative cell viability (%).

Statistical Analysis

Statistical analyses were performed with an unpaired Student *t* test for experiments with two groups (GraphPad Prism). One-way ANOVA was used to compare multiple experimental groups, and two-way ANOVA was used to compare continuous outcomes across multiple experimental groups. For all tests, $P < 0.05$ was considered significant. Sample size was not predetermined. Unless noted, samples were independent biological replicates.

Disclosure of Potential Conflicts of Interest

E.M. Stone is a consultant for and has equity interest in Aeglea Biotherapeutics, and is an inventor on intellectual property related to this work owned by The University of Texas at Austin. G. Georgiou has ownership interest (including patents) in Aeglea Biotherapeutics. M.A. Morgan is an advisory board member for AstraZeneca, reports receiving a commercial research grant from AstraZeneca, and has received honoraria from the speakers' bureau of AstraZeneca. W. Zou is a scientific board member at EMD, Cstone, Synlogic, and Henlius. No potential conflicts of interest were disclosed by the other authors.

Authors' Contributions

Conception and design: X. Lang, M.D. Green, T.S. Lawrence, W. Zou
Development of methodology: X. Lang, M.D. Green, W. Wang, L. Jiang, Q. Zhang, I. Kryczek
Acquisition of data (provided animals, acquired and managed patients, provided facilities, etc.): X. Lang, M.D. Green, W. Wang, J. Yu, A. Dow, A.L. Saripalli, S. Wei, E.M. Stone, T.S. Lawrence
Analysis and interpretation of data (e.g., statistical analysis, biostatistics, computational analysis): X. Lang, M.D. Green, W. Wang, J.E. Choi, G. Georgiou, M. Cieslik, M.A. Morgan, A.M. Chinnaiyan, T.S. Lawrence, W. Zou
Writing, review, and/or revision of the manuscript: X. Lang, M.D. Green, A.L. Saripalli, G. Georgiou, D.R. Wahl, M.A. Morgan, A.M. Chinnaiyan, T.S. Lawrence, W. Zou
Administrative, technical, or material support (i.e., reporting or organizing data, constructing databases): M.D. Green, P. Liao, J. Zhou, Q. Zhang, S. Wei, W. Szeliga, L. Vatan, G. Georgiou, A.M. Chinnaiyan, W. Zou
Study supervision: M.D. Green, W. Zou

Acknowledgments

This work was supported in part by research grants from the NIH/NCI for W. Zou (CA217648, CA123088, CA099985, CA193136, and CA152470), E.M. Stone and G. Georgiou (CA189623), T.S. Lawrence (U01CA216440), and A.M. Chinnaiyan (1UM1HG006508); and the NIH through the University of Michigan Rogel Cancer Center Support Grant (P30CA46592). The authors would like to thank all members of the Zou lab for their insightful feedback, as well as acknowledge the support of the University of Michigan Experimental Irradiation Shared Resource, the Research Histology and Immunohistochemistry Core, and the Advanced Genomics Core.

The costs of publication of this article were defrayed in part by the payment of page charges. This article must therefore be hereby marked *advertisement* in accordance with 18 U.S.C. Section 1734 solely to indicate this fact.

Received March 17, 2019; revised August 5, 2019; accepted September 20, 2019; published first September 25, 2019.

REFERENCES

1. Zou W, Wolchok JD, Chen L. PD-L1 (B7-H1) and PD-1 pathway blockade for cancer therapy: mechanisms, response biomarkers and combinations. Sci Transl Med 2016;8:328rv4.
2. Kang J, Demaria S, Formenti S. Current clinical trials testing the combination of immunotherapy with radiotherapy. J Immunother Cancer 2016;4:51.
3. Harding SM, Benci JL, Irianto J, Discher DE, Minn AJ, Greenberg RA. Mitotic progression following DNA damage enables pattern recognition within micronuclei. Nature 2017;548:466–70.
4. Vanpouille-Box C, Alard A, Aryankalayil MJ, Sarfraz Y, Diamond JM, Schneider RJ, et al. DNA exonuclease Trex1 regulates radiotherapy-induced tumour immunogenicity. Nat Commun 2017;8:15618.
5. Bakhoum SF, Kabeche L, Wood MD, Laucius CD, Qu D, Laughney AM, et al. Numerical chromosomal instability mediates susceptibility to radiation treatment. Nat Commun 2015;6:5990.
6. Morgan MA, Lawrence TS. Molecular pathways: overcoming radiation resistance by targeting DNA damage response pathways. Clin Cancer Res 2015;21:2898–904.
7. Chan TA, Hermeking H, Lengauer C, Kinzler KW, Vogelstein B. 14-3-3σ is required to prevent mitotic catastrophe after DNA damage. Nature 1999;401:616.
8. Wang H-H, Wu Z-Q, Qian D, Zaorsky NG, Qiu M-H, Cheng J-J, et al. Ablative hypofractionated radiation therapy enhances non-small cell lung cancer cell killing via preferential stimulation of necroptosis in vitro and in vivo. Int J Radiat Oncol Biol Phys 2018;101:49–62.
9. Okada H, Mak TW. Pathways of apoptotic and non-apoptotic death in tumour cells. Nat Rev Cancer 2004;4:592.
10. Gebicki JM, Du J, Collins J, Tweeddale H. Peroxidation of proteins and lipids in suspensions of liposomes, in blood serum, and in mouse myeloma cells. Acta Biochim Pol 2000;47:901–11.
11. Spitz DR, Azzam EI, Li JJ, Gius D. Metabolic oxidation/reduction reactions and cellular responses to ionizing radiation: a unifying concept in stress response biology. Cancer Metastasis Rev 2004;23:311–22.
12. Dixon SJ, Lemberg KM, Lamprecht MR, Skouta R, Zaitsev EM, Gleason CE, et al. Ferroptosis: an iron-dependent form of nonapoptotic cell death. Cell 2012;149:1060–72.
13. Haimovitz-Friedman A, Kan CC, Ehleiter D, Persaud RS, McLoughlin M, Fuks Z, et al. Ionizing radiation acts on cellular membranes to generate ceramide and initiate apoptosis. J Exp Med 1994;180:525–35.
14. Deng L, Liang H, Xu M, Yang X, Burnette B, Arina A, et al. STING-dependent cytosolic DNA sensing promotes radiation-induced type I interferon-dependent antitumor immunity in immunogenic tumors. Immunity 2014;41:843–52.
15. Deng L, Liang H, Burnette B, Beckett M, Darga T, Weichselbaum RR, et al. Irradiation and anti-PD-L1 treatment synergistically promote antitumor immunity in mice. J Clin Invest 2014;124:687–95.
16. Wang W, Green M, Choi JE, Gijón M, Kennedy PD, Johnson JK, et al. CD8+ T cells regulate tumour ferroptosis during cancer immunotherapy. Nature 2019;569:270.
17. Yang WS, Stockwell BR. Ferroptosis: death by lipid peroxidation. Trends Cell Biol 2015;26:165–176.
18. Cramer SL, Saha A, Liu J, Tadi S, Tiziani S, Yan W, et al. Systemic depletion of L-cyst(e)ine with cyst(e)inase increases reactive oxygen species and suppresses tumor growth. Nat Med 2016;23:120.
19. Magtanong L, Ko PJ, To M, Cao JY, Forcina GC, Tarangelo A, et al. Exogenous monounsaturated fatty acids promote a ferroptosis-resistant cell state. Cell Chem Biol 2019;26:420–32.e9.
20. Doll S, Proneth B, Tyurina YY, Panzilius E, Kobayashi S, Ingold I, et al. ACSL4 dictates ferroptosis sensitivity by shaping cellular lipid composition. Nat Chem Biol 2016;13:91.
21. Lee Y, Auh SL, Wang Y, Burnette B, Wang Y, Meng Y, et al. Therapeutic effects of ablative radiation on local tumor require CD8+ T cells: changing strategies for cancer treatment. Blood 2009;114:589–95.
22. Minn AJ, Wherry EJ. Combination cancer therapies with immune checkpoint blockade: convergence on interferon signaling. Cell 2016;165:272–5.
23. Poli G, Schaur RJ, Siems WA, Leonarduzzi G. 4-Hydroxynonenal: a membrane lipid oxidation product of medicinal interest. Med Res Rev 2008;28:569–631.
24. Peng D, Kryczek I, Nagarsheth N, Zhao L, Wei S, Wang W, et al. Epigenetic silencing of TH1-type chemokines shapes tumour immunity and immunotherapy. Nature 2015;527:249–53.
25. Venkata Narayanan I, Paulsen MT, Bedi K, Berg N, Ljungman EA, Francia S, et al. Transcriptional and post-transcriptional regulation of the ionizing radiation response by ATM and p53. Sci Rep 2017;7:43598.
26. Dixon SJ, Patel DN, Welsch M, Skouta R, Lee ED, Hayano M, et al. Pharmacological inhibition of cystine–glutamate exchange induces endoplasmic reticulum stress and ferroptosis. Elife 2014;3:e02523.
27. Yang WS, SriRamaratnam R, Welsch ME, Shimada K, Skouta R, Viswanathan VS, et al. Regulation of ferroptotic cancer cell death by GPX4. Cell 2014;156:317–31.
28. Purbey PK, Scumpia PO, Kim PJ, Tong A-J, Iwamoto KS, McBride WH, et al. Defined sensing mechanisms and signaling pathways contribute to the global inflammatory gene expression output elicited by ionizing radiation. Immunity 2017;47:421–34.e3.
29. Chen P-H, Wu J, Ding C-KC, Lin C-C, Pan S, Bossa N, et al. Kinome screen of ferroptosis reveals a novel role of ATM in regulating iron metabolism. Cell Death Differ 2019 Jul 18 [Epub ahead of print].
30. Banin S, Moyal L, Shieh S-Y, Taya Y, Anderson C, Chessa L, et al. Enhanced phosphorylation of p53 by ATM in response to DNA damage. Science 1998;281:1674–7.

31. Wang W, Kryczek I, Dostál L, Lin H, Tan L, Zhao L, et al. Effector T cells abrogate stroma-mediated chemoresistance in ovarian cancer. Cell 2016;165:1092–105.
32. Dewan MZ, Galloway AE, Kawashima N, Dewyngaert JK, Babb JS, Formenti SC, et al. Fractionated but not single-dose radiotherapy induces an immune-mediated abscopal effect when combined with anti-CTLA-4 antibody. Clin Cancer Res 2009;15:5379–88.
33. Twyman-Saint Victor C, Rech AJ, Maity A, Rengan R, Pauken KE, Stelekati E, et al. Radiation and dual checkpoint blockade activate non-redundant immune mechanisms in cancer. Nature 2015;520:373–7.
34. Stockwell BR, Friedmann Angeli JP, Bayir H, Bush AI, Conrad M, Dixon SJ, et al. Ferroptosis: a regulated cell death nexus linking metabolism, redox biology, and disease. Cell 2017;171:273–85.
35. Kruiswijk F, Labuschagne C, Vousden K, p53 in survival, death and metabolic health: a lifeguard with a licence to kill. Nat Rev Mol Cell Biol 2015;16:393–405.
36. Durant ST, Zheng L, Wang Y, Chen K, Zhang L, Zhang T, et al. The brain-penetrant clinical ATM inhibitor AZD1390 radiosensitizes and improves survival of preclinical brain tumor models. Sci Adv 2018;4:eaat1719.
37. Pardoll DM. The blockade of immune checkpoints in cancer immunotherapy. Nat Rev Cancer 2012;12:252–64.
38. Ribas A. Adaptive immune resistance: how cancer protects from immune attack. Cancer Discov 2015;5:915–9.
39. Curiel TJ, Wei S, Dong H, Alvarez X, Cheng P, Mottram P, et al. Blockade of B7-H1 improves myeloid dendritic cell–mediated antitumor immunity. Nat Med 2003;9:562–7.
40. Lin H, Wei S, Hurt EM, Green MD, Zhao L, Vatan L, et al. Host expression of PD-L1 determines efficacy of PD-L1 pathway blockade–mediated tumor regression. J Clin Invest 2018;128:805–15.
41. Curiel TJ, Coukos G, Zou L, Alvarez X, Cheng P, Mottram P, et al. Specific recruitment of regulatory T cells in ovarian carcinoma fosters immune privilege and predicts reduced survival. Nat Med 2004;10:942–9.
42. Karnak D, Engelke CG, Parsels LA, Kausar T, Wei D, Robertson JR, et al. Combined inhibition of Wee1 and PARP1/2 for radiosensitization in pancreatic cancer. Clin Cancer Res 2014;20:5085–96.
43. Robinson MD, McCarthy DJ, Smyth GK. edgeR: a Bioconductor package for differential expression analysis of digital gene expression data. Bioinformatics 2010;26:139–40.